

A measurement of the CP asymmetry difference between $\Lambda_c^+ \rightarrow pK^-K^+$ and $p\pi^-\pi^+$ decays



The LHCb collaboration

E-mail: alex.pearce@cern.ch

ABSTRACT: The difference between the CP asymmetries in the decays $\Lambda_c^+ \rightarrow pK^-K^+$ and $\Lambda_c^+ \rightarrow p\pi^-\pi^+$ is presented. Proton-proton collision data taken at centre-of-mass energies of 7 and 8 TeV collected by the LHCb detector in 2011 and 2012 are used, corresponding to an integrated luminosity of 3 fb^{-1} . The Λ_c^+ candidates are reconstructed as part of the $\Lambda_b^0 \rightarrow \Lambda_c^+ \mu^- X$ decay chain. In order to maximize the cancellation of production and detection asymmetries in the difference, the final-state kinematic distributions of the two samples are aligned by applying phase-space-dependent weights to the $\Lambda_c^+ \rightarrow p\pi^-\pi^+$ sample. This alters the definition of the integrated CP asymmetry to $A_{CP}^{\text{wgt}}(p\pi^-\pi^+)$. Both samples are corrected for reconstruction and selection efficiencies across the five-dimensional Λ_c^+ decay phase space. The difference in CP asymmetries is found to be

$$\begin{aligned} \Delta A_{CP}^{\text{wgt}} &= A_{CP}(pK^-K^+) - A_{CP}^{\text{wgt}}(p\pi^-\pi^+) \\ &= (0.30 \pm 0.91 \pm 0.61) \%, \end{aligned}$$

where the first uncertainty is statistical and the second is systematic.

KEYWORDS: Charm physics, CP violation, Flavor physics, Hadron-Hadron scattering (experiments)

ARXIV EPRINT: [1712.07051](https://arxiv.org/abs/1712.07051)

Contents

1	Introduction	1
2	Formalism	2
3	Detector and dataset	4
4	Mass spectrum parameterisation	5
5	Kinematic and efficiency corrections	7
5.1	Kinematic weighting	7
5.2	Efficiency corrections	8
5.3	Use in determining A_{raw}	8
6	Systematic effects	10
7	Results	11
8	Summary	12
	The LHCb collaboration	16

1 Introduction

The Standard Model (SM) does not provide a source of charge-parity (CP) symmetry violation large enough to explain the matter-antimatter asymmetry observed in the universe [1]. The ongoing experimental effort in searching for CP violation in particle decays aims to find effects that are not expected in the SM, such that new dynamics are required. Whilst the existence of CP violation in kaon and beauty meson decays is well established [2, 3], no observation has been made in the analyses of beauty baryons or charm hadrons, although evidence of CP violation has recently been claimed for the former [4]. The most precise searches for CP violation in the charm sector have been made using self-conjugate, singly Cabibbo-suppressed (SCS) decays of the neutral D^0 meson to K^-K^+ and $\pi^-\pi^+$ final states [5, 6]. Such SCS decays can include significant contributions from loop-level amplitudes, within which new dynamics can enter.

This article reports a search for CP violation in the decays of the Λ_c^+ charm baryon to the SCS pK^-K^+ and $p\pi^-\pi^+$ final states (generically referred to as ph^-h^+).¹ The difference in CP asymmetry between the two decays, ΔA_{CP} , is measured in a manner similar to previous measurements using D^0 decays [5, 6]. There is little theoretical understanding of

¹Charge conjugation is implied throughout this article, except in the definition of asymmetry terms.

the dynamics of $\Lambda_c^+ \rightarrow ph^-h^+$ decays [7], partly due to the unknown resonant structure of the five-dimensional (5D) phase space and partly due to the historical lack of large experimental datasets, and so no predictions for the magnitude of CP violation in $\Lambda_c^+ \rightarrow ph^-h^+$ decays are currently available. As CP violation may be dependent on the position in phase space, leading to locally significant effects, a multidimensional analysis would be required to be maximally sensitive to such behaviour, requiring assumptions on the as-yet unknown amplitude model and Λ_c^+ polarisation. The work presented here instead integrates over the phase space as a search for global CP -violating effects.

The presented analysis uses proton-proton collision data taken at centre-of-mass energies of $\sqrt{s} = 7$ TeV and 8 TeV, collected by the LHCb experiment at the Large Hadron Collider (LHC) in 2011 and 2012, corresponding to an integrated luminosity of 3 fb^{-1} . To reduce the level of backgrounds, candidate $\Lambda_c^+ \rightarrow ph^-h^+$ decays are reconstructed as part of the $\Lambda_b^0 \rightarrow \Lambda_c^+ \mu^- X$ decay chain, where X represents any number of additional, unreconstructed particles. The long lifetime of the Λ_b^0 baryon [2], in comparison with that of the Λ_c^+ baryon, allows for the suppression of backgrounds through the requirement of a $\Lambda_c^+ \mu^-$ vertex that is displaced with respect to the primary pp interaction. The total dataset contains of the order of 10^4 and 10^5 reconstructed pK^-K^+ and $p\pi^-\pi^+$ signal candidates, respectively.

The observed charge asymmetry $A_{\text{raw}}(f)$ for each Λ_c^+ final state f , reconstructed in association with a muon, is measured as the difference in Λ_c^+ and $\bar{\Lambda}_c^-$ signal yields divided by their sum. The quantity A_{raw} includes contributions from the CP asymmetry in the Λ_c^+ decay, as well as asymmetries due to experimental effects such as the Λ_b^0 production asymmetry and the muon and hadron detection asymmetries. These effects have been measured at LHCb [5, 8–10], but with large uncertainties. Using them directly, to correct for the experimental asymmetries in A_{raw} , would then result in large systematic uncertainties on the correction factors. Instead, assuming that the asymmetries are, or can be made to be, mode independent, the difference $\Delta A_{CP} = A_{\text{raw}}(pK^-K^+) - A_{\text{raw}}(p\pi^-\pi^+)$ is equal to the difference in the Λ_c^+ decay asymmetries, as all other asymmetries cancel. A weighting technique is used to equalise the pK^-K^+ and $p\pi^-\pi^+$ sample kinematics, thereby improving the level of cancellation of the various production, reconstruction, and selection asymmetries in ΔA_{CP} , the formalism for which is presented in section 2. A description of the LHCb detector and the analysis dataset is given in section 3, followed by a description of the statistical models used to determine the signal yields from the data in section 4. The weighting method used for correcting the measurement for experimental asymmetries and the evaluation of the efficiency variation across the 5D ph^-h^+ phase space are presented in section 5. Systematic effects are considered and quantified in section 6. The results of the analysis are given in section 7, and finally a summary is made in section 8.

2 Formalism

The CP asymmetry in the decays of the Λ_c^+ baryon to a given final state f is

$$A_{CP}(f) = \frac{\Gamma(f) - \Gamma(\bar{f})}{\Gamma(f) + \Gamma(\bar{f})}, \quad (2.1)$$

where $\Gamma(f)$ is the decay rate of the $\Lambda_c^+ \rightarrow f$ process, and $\Gamma(\bar{f})$ is the decay rate of the charge conjugate decay $\bar{\Lambda}_c^- \rightarrow \bar{f}$. Rather than measure the individual decay rates, it is simpler to count the number of reconstructed decays, and so the asymmetry in the yields is defined as

$$A_{\text{raw}}(f) = \frac{N(f\mu^-) - N(\bar{f}\mu^+)}{N(f\mu^-) + N(\bar{f}\mu^+)}, \quad (2.2)$$

where N is the number of signal candidates reconstructed in association with a muon. This is labelled as the raw asymmetry of the decay because the measurement of the physics observable of interest, A_{CP} , is contaminated by several experimental asymmetries. Assuming that each contributing factor is small, the raw asymmetry can be expressed to first order as the sum

$$A_{\text{raw}}(f) = A_{CP}(f) + A_P^{A_b^0}(f\mu) + A_D^\mu(\mu) + A_D^f(f), \quad (2.3)$$

where $A_P^{A_b^0}$, A_D^μ , and A_D^f are the A_b^0 production asymmetry, muon detection asymmetry, and Λ_c^+ final-state detection asymmetry, respectively. A nonzero A_b^0 production asymmetry may arise for several reasons, such as the relative abundance of matter quarks in the pp collision region. A dependence on the reconstructed A_b^0 final state is introduced by the detector acceptance and the reconstruction and selection applied to that state, which alters the observed A_b^0 production phase space. The two detection asymmetries may be nonzero due to the different interaction cross-sections of the matter and antimatter states with the LHCb detector. There may also be charge-dependent reconstruction and selection effects. In all cases, an experimental asymmetry is assumed to be fully parameterised by the kinematics of the objects involved. The asymmetry of interest, A_{CP} , is assumed to be dependent on f but independent of Λ_c^+ kinematics. This motivates a measurement of the difference between raw asymmetries of two distinct Λ_c^+ decay modes, chosen to be pK^-K^+ and $p\pi^-\pi^+$ in this analysis,

$$\Delta A_{CP} = A_{CP}(pK^-K^+) - A_{CP}(p\pi^-\pi^+) \quad (2.4)$$

$$\approx A_{\text{raw}}(pK^-K^+) - A_{\text{raw}}(p\pi^-\pi^+), \quad (2.5)$$

where the approximation tends to an equality as the kinematics between the final states become indistinguishable.

The observed kinematics of the $pK^-K^+\mu^-$ and $p\pi^-\pi^+\mu^-$ final states are not expected to be equal given the different energy release and resonant structure of the two Λ_c^+ decays. To ensure similarity, the kinematic spectra of one state can be matched to that of another. As around six times as many $p\pi^-\pi^+$ signal candidates are found than pK^-K^+ signal candidates, as described in section 4, the $p\pi^-\pi^+\mu^-$ data are weighted to match the $pK^-K^+\mu^-$ data, given that the statistical uncertainty on the $A_{\text{raw}}(pK^-K^+)$ measurement will be the dominant contribution to that on $\Delta A_{CP}^{\text{wgt}}$. Details of the weighting procedure are given in section 5. The kinematic weighting may alter the physics asymmetry, as the $p\pi^-\pi^+$ phase space can be distorted, and so it is a weighted asymmetry, A_{CP}^{wgt} , that enters the measurement

$$\Delta A_{CP}^{\text{wgt}} = A_{CP}(pK^-K^+) - A_{CP}^{\text{wgt}}(p\pi^-\pi^+) \quad (2.6)$$

$$\approx A_{\text{raw}}(pK^-K^+) - A_{\text{raw}}^{\text{wgt}}(p\pi^-\pi^+). \quad (2.7)$$

To allow for comparisons with theoretical models, a weighting function is provided in the supplementary material of this article which provides a weight for a given coordinate in the five-dimensional $\Lambda_c^+ \rightarrow p\pi^-\pi^+$ phase space and mimics the transformation imposed by the kinematic weighting applied here. The five dimensions are defined similarly to those in ref. [11], with the only difference being that the ‘beam axis’ is replaced by the displacement vector pointing from the pp collision vertex, the primary vertex (PV), to the $\Lambda_c^+\mu^-$ vertex.

3 Detector and dataset

The LHCb detector [12, 13] is a single-arm forward spectrometer covering the pseudorapidity range $2 < \eta < 5$, designed for the study of particles containing b or c quarks. The detector includes a high-precision tracking system consisting of a silicon-strip vertex detector surrounding the pp interaction region, a large-area silicon-strip detector located upstream of a dipole magnet with a bending power of about 4 T m, and three stations of silicon-strip detectors and straw drift tubes placed downstream of the magnet. The tracking system provides a measurement of the momentum of charged particles with a relative uncertainty that varies from 0.5% at low momentum to 1.5% at 200 GeV/ c . The minimum distance of a track to a PV, the impact parameter, is measured with a resolution of $(15 + 29/p_T)$ μm , where p_T is the component of the momentum transverse to the beam, in GeV/ c . Different types of charged hadrons are distinguished using information from two ring-imaging Cherenkov detectors. Photons, electrons, and hadrons are identified by a calorimeter system consisting of scintillating-pad and preshower detectors, an electromagnetic calorimeter, and a hadronic calorimeter. Muons are identified by a system composed of alternating layers of iron and multiwire proportional chambers. To control possible left-right interaction asymmetries, the polarity of the dipole magnet is reversed periodically throughout data-taking. The configuration with the magnetic field vertically upwards (downwards) bends positively (negatively) charged particles in the horizontal plane towards the centre of the LHC.

The online event selection is performed by a trigger, which consists of a hardware stage, based on information from the calorimeter and muon systems, followed by a two-stage software trigger, which applies first a simplified and then a full event reconstruction. For the dataset used for the present analysis, at the hardware trigger stage the presence of a high- p_T muon candidate is required. In the first stage of the software trigger, this candidate must be matched to a good-quality track which is inconsistent with originating directly from any PV and has a p_T above 1 GeV/ c . The second stage requires a two-, three-, or four-track secondary vertex with a significant displacement from all PVs, where at least one of the tracks is consistent with being a muon. At least one charged particle must have $p_T > 1.6$ GeV/ c and must be inconsistent with originating from any PV. A multivariate algorithm [14] is used for the identification of secondary vertices consistent with the decays of beauty hadrons.

In the offline selection, tracks are selected on the criteria that they have a significant impact parameter with respect to all PVs, and also on the particle identification information being consistent with one of the proton, kaon, or pion hypotheses. Sets of three tracks with

$\sum p_T > 1.8 \text{ GeV}/c$ are combined to form Λ_c^+ candidates. Each candidate is required to be displaced significantly from all PVs, to have a good quality vertex, and to have an invariant mass between 2230 and 2350 MeV/c^2 . The Λ_c^+ candidate is combined with a displaced muon to form the Λ_b^0 candidate, which must have a good quality vertex and also satisfy the invariant mass requirement $2.5 < m(\Lambda_c^+ \mu^-) < 6 \text{ GeV}/c^2$. The offline Λ_b^0 candidate is required to be matched to the candidate formed in the second stage of the software trigger.

Contributions from the Cabibbo-favoured decays $\Lambda_c^+ \rightarrow p\bar{K}^0$ and $\Lambda_c^+ \rightarrow \Lambda\pi^+$, and their charge conjugates, are observed in the background-subtracted $m(\pi^-\pi^+)$ and $m(p\pi^-)$ spectra. These are removed by applying a veto in the two-pion invariant mass spectrum $485 < m(\pi^-\pi^+) < 510 \text{ MeV}/c^2$ to remove K_S^0 meson contributions, and in the proton-pion invariant mass spectrum $1110 < m(p\pi^-) < 1120 \text{ MeV}/c^2$ to remove Λ baryons. Contributions from misidentified charm meson and background Λ_c^+ decays are removed by applying a $16 \text{ MeV}/c^2$ wide veto centred on the world average mass value [2] for the charm hadron in question. Such vetoes are applied in the misidentified mass distributions for the following backgrounds: $D^+ \rightarrow K^-K^+\pi^+$, $D_s^+ \rightarrow K^-K^+\pi^+$, and $\Lambda_c^+ \rightarrow pK^-\pi^+$ for pK^-K^+ candidates; and $D^+ \rightarrow K^-\pi^+\pi^+$, $D^+ \rightarrow K^-K^+\pi^+$, $D_s^+ \rightarrow K^-K^+\pi^+$, and $D_s^+ \rightarrow \pi^-K^+\pi^+$ for $p\pi^-\pi^+$ candidates.

After the selection, less than 2% of the events contain more than one Λ_b^0 candidate. All candidates are kept for the rest of the analysis, as other techniques of dealing with multiple candidates per event have been shown to be biased for asymmetry measurements [15].

The data were taken at two centre-of-mass energies, $\sqrt{s} = 7 \text{ TeV}$ in 2011 and 8 TeV in 2012, and with two configurations of the dipole magnet polarity. As the experimental efficiencies vary with these conditions, due to different momentum production spectra and the left-right asymmetries in the detector construction, the data are split into four independent subsamples by centre-of-mass-energy and magnet polarity. Each stage of the analysis is carried out on each subsample independently, and then the individual results are combined in an average as described in section 7.

Simulated pp collisions are used to determine experimental efficiencies and are generated using PYTHIA [16, 17] with a specific LHCb configuration [18]. Particle decays are described by EVTGEN [19], in which final-state radiation is generated using PHOTOS [20]. The interaction of the generated particles with the detector, and its response, are implemented using the GEANT4 toolkit [21, 22] as described in ref. [23].

4 Mass spectrum parameterisation

The ph^-h^+ invariant mass is used as a discriminating variable between signal and combinatorial background. Fits to the mass spectrum, shown in figure 1, are used to measure the ph^-h^+ signal yields in order to compute A_{raw} , as defined in eq. (2.2). The sPlot procedure [24] is employed to statistically subtract the combinatorial background component in the data, as required for the kinematic weighting procedure, and takes the fitted model as input.

The chosen fit model is the sum of a signal component and a background component, each weighted by a corresponding yield parameter. The signal is modelled as the sum of two

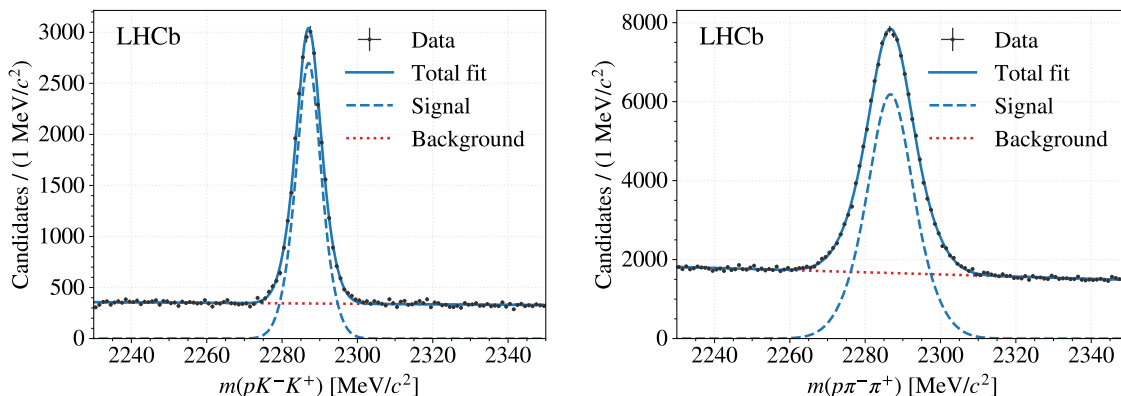


Figure 1. The ph^-h^+ invariant mass spectra from the fully selected $\Lambda_c^+ \rightarrow pK^-K^+$ (left) and $\Lambda_c^+ \rightarrow p\pi^-\pi^+$ (right) datasets summed over all data-taking conditions. The results of the fit to each dataset are shown for illustration. The widths of the signal distributions differ due to the different Q -value between the two decays, where the larger value for the $\Lambda_c^+ \rightarrow p\pi^-\pi^+$ mode results in a broader shape.

\sqrt{s}	Polarity	Int. lumi. [pb^{-1}]	pK^-K^+ yield	$p\pi^-\pi^+$ yield
7 TeV	Up	422 ± 7	2880 ± 70	$18\,450 \pm 190$
7 TeV	Down	563 ± 9	3940 ± 80	$25\,130 \pm 230$
8 TeV	Up	1000 ± 11	9040 ± 120	$57\,730 \pm 350$
8 TeV	Down	992 ± 11	9330 ± 120	$60\,080 \pm 360$

Table 1. Signal yields measured in the fit for each of the four subsets of the pK^-K^+ and $p\pi^-\pi^+$ data (two centre-of-mass energies, 7 and 8 TeV, and two polarities of the dipole magnet, up and down). The corresponding integrated luminosity of each subset is also given.

Gaussian distributions which share a common mean but have separate width parameters, and the combinatorial background is modelled as a first-order polynomial.

A cost function is defined as Neyman’s χ^2 ,

$$\chi^2 = \sum_{i=1}^B \frac{(N_i - N f_{\text{Tot}}(m_i; \xi))^2}{N_i}, \quad (4.1)$$

where i is the bin index over the number of bins B in the $m(ph^-h^+)$ spectrum, N_i is the observed number of entries in the i th bin, N is the expected number of entries in the dataset as the sum of the fitted signal and background yield parameters, and $f_{\text{Tot}}(m_i; \xi)$ represents the integral of the total model in the m_i bin with parameter vector ξ . The binning is set as 120 bins of width $1 \text{ MeV}/c^2$ in the range $2230 < m(ph^-h^+) < 2350 \text{ MeV}/c^2$. Fits to the pK^-K^+ and $p\pi^-\pi^+$ data, summed over all conditions, are shown in figure 1. A good description of the data by the model is seen in all fits to the data subsamples. The pK^-K^+ and $p\pi^-\pi^+$ signal yields, separated by data-taking conditions, are given in table 1.

To measure A_{raw} as in eq. (2.2), each data subsample is split by proton charge into Λ_c^+ and $\bar{\Lambda}_c^-$ subsets. The model used in the previously described fit is used to define charge-

dependent models, where the parameter vectors of each model, ξ^+ and ξ^- , are independent. Rather than fitting charge-dependent signal and background yields directly, however, they are parameterised using the total number of signal and background candidates, N_{Sig} and N_{Bkg} , and the signal and background asymmetries, A_{raw} and $A_{\text{raw}}^{\text{Bkg}}$,

$$N_{\text{Sig}}^{\pm} = \frac{1}{2} N_{\text{Sig}} (1 \pm A_{\text{raw}}), \tag{4.2}$$

$$N_{\text{Bkg}}^{\pm} = \frac{1}{2} N_{\text{Bkg}} (1 \pm A_{\text{raw}}^{\text{Bkg}}). \tag{4.3}$$

The addition of per-candidate weights, which are described in the following section, requires a cost function that uses the sum of weights in each bin, rather than the count as in eq. (4.1), defined as

$$\chi^2 = \sum_{i=1}^B \left[\frac{(W_i^+ - N^+ f_{\text{Tot}}^+(m_i; \xi^+))^2}{(\delta W_i^+)^2} + \frac{(W_i^- - N^- f_{\text{Tot}}^-(m_i; \xi^-))^2}{(\delta W_i^-)^2} \right], \tag{4.4}$$

where W_i^{\pm} is the sum of the weights of candidates in the i th bin in the A_c^{\pm} sample, and δW_i^{\pm} is the uncertainty on that sum.

5 Kinematic and efficiency corrections

The experimental asymmetries listed in eq. (2.3) are specific to the production environment at the LHC and the construction of the LHCb detector, and so their cancellation in $\Delta A_{CP}^{\text{wgt}}$ is crucial in providing an unbiased measurement. This section presents the statistical methods used to compute the kinematic and efficiency corrections, which are evaluated as per-candidate weights to be used in the simultaneous χ^2 fit previously described.

5.1 Kinematic weighting

The production and detection asymmetries depend on the kinematics of the particles involved. If the A_b^0 , muon, and proton kinematic spectra are the same between the pK^-K^+ and $p\pi^-\pi^+$ data, then the A_b^0 production asymmetry and muon and proton detection asymmetries will cancel in $\Delta A_{CP}^{\text{wgt}}$. If the h^- and h^+ kinematics are equal *within* each separate pK^-K^+ and $p\pi^-\pi^+$ sample, then the kaon ($f = pK^-K^+$) or pion ($f = p\pi^-\pi^+$) detection asymmetries will cancel in $A_{\text{raw}}(f)$. The h^- kinematics agree well with the h^+ spectra in the data, but the A_b^0 , muon, and proton kinematics do not, and so a per-candidate weighting technique is employed to match the kinematic spectra of the $p\pi^-\pi^+\mu^-$ state to those of the $pK^-K^+\mu^-$ state.

To compute the per-candidate weights, a forest of shallow decision trees with gradient boosting (a GBDT) is used [25–27]. This method recursively bins the pK^-K^+ and $p\pi^-\pi^+$ input data such that regions with larger differences between the two samples are more finely partitioned. After fitting, each $p\pi^-\pi^+$ candidate is assigned a weight d . To reduce biases that may result from overfitting, where the GBDT model becomes sensitive to the statistical fluctuations in the input data, the data are split in two, and independent GBDTs are fitted to each subset. The GBDT built with one half of the data is used to evaluate weights for the other half, and vice versa.

The Λ_c^+ and proton p_T and pseudorapidity for each pK^-K^+ and $p\pi^-\pi^+$ candidate are used as input to the GBDT. The Λ_c^+ kinematics are chosen since the large boost in the laboratory frame induces a large correlation with Λ_b^0 and muon kinematics. An agreement in the Λ_c^+ kinematics therefore results in an agreement in the Λ_b^0 and muon spectra. The proton kinematics are chosen as the different Q values of the decays will a priori result in different proton spectra.

The Λ_b^0 , muon, proton, and h^-/h^+ kinematics agree well after weighting, as demonstrated for a subset of kinematic variables in figure 2. Any remaining differences will result in residual asymmetries in $\Delta A_{CP}^{\text{wgt}}$, and the presence of these differences is studied in the context of systematic effects as described in section 6.

5.2 Efficiency corrections

The acceptance, reconstruction, and selection efficiencies as a function of the 5D ph^-h^+ phase space are also modelled using GBDTs. Simulated events are generated with a uniform $\Lambda_c^+ \rightarrow ph^-h^+$ matrix element and used as input to the training, sampled before and after the detector acceptance and data processing steps. One- and two-dimensional efficiency estimates are made as histogram ratios of the before and after data, and projections of the efficiency model obtained using the simulation agrees well with these. The model is then used to predict per-candidate efficiencies in the data.

5.3 Use in determining A_{raw}

The cost function in eq. (4.4) uses the sum of per-candidate weights in each bin and its uncertainty. The weights are defined using the kinematic weight d_j , equal to unity for $\Lambda_c^+ \rightarrow pK^-K^+$ candidates, and the efficiency correction ε_j of the j th candidate in the i th $m(ph^-h^+)$ bin,

$$W_i = W \sum_{j=1}^{N_i} \frac{d_j}{\varepsilon_j}, \quad \delta W_i^2 = W_i, \quad (5.1)$$

where the normalisation factor W is defined as

$$W = \frac{\sum_{j=1}^{N_i} \frac{d_j}{\varepsilon_j}}{\sum_{j=1}^{N_i} \left(\frac{d_j}{\varepsilon_j}\right)^2}. \quad (5.2)$$

The term W_i can be called the number of ‘effective’ entries in the bin, as it encodes the size of an unweighted data sample with the same statistical power as the weighted sample. For the $p\pi^-\pi^+$ data, which is weighted to match the pK^-K^+ kinematics, the effective sample size is around 80% that of the unweighted $p\pi^-\pi^+$ sample. The weighted data are shown in the $m^2(ph^-)-m^2(h^-h^+)$ plane in figure 3.

The statistical treatment of the weights in the fit is validated by randomly sorting candidates into Λ_c^+ and $\bar{\Lambda}_c^-$ datasets and fitting the model 500 times, where it is seen that the distribution of $A_{\text{raw}}(f)$ divided by its uncertainty is centred around zero, the expected value, and has a standard deviation of 1, indicating that the error estimate is correct.

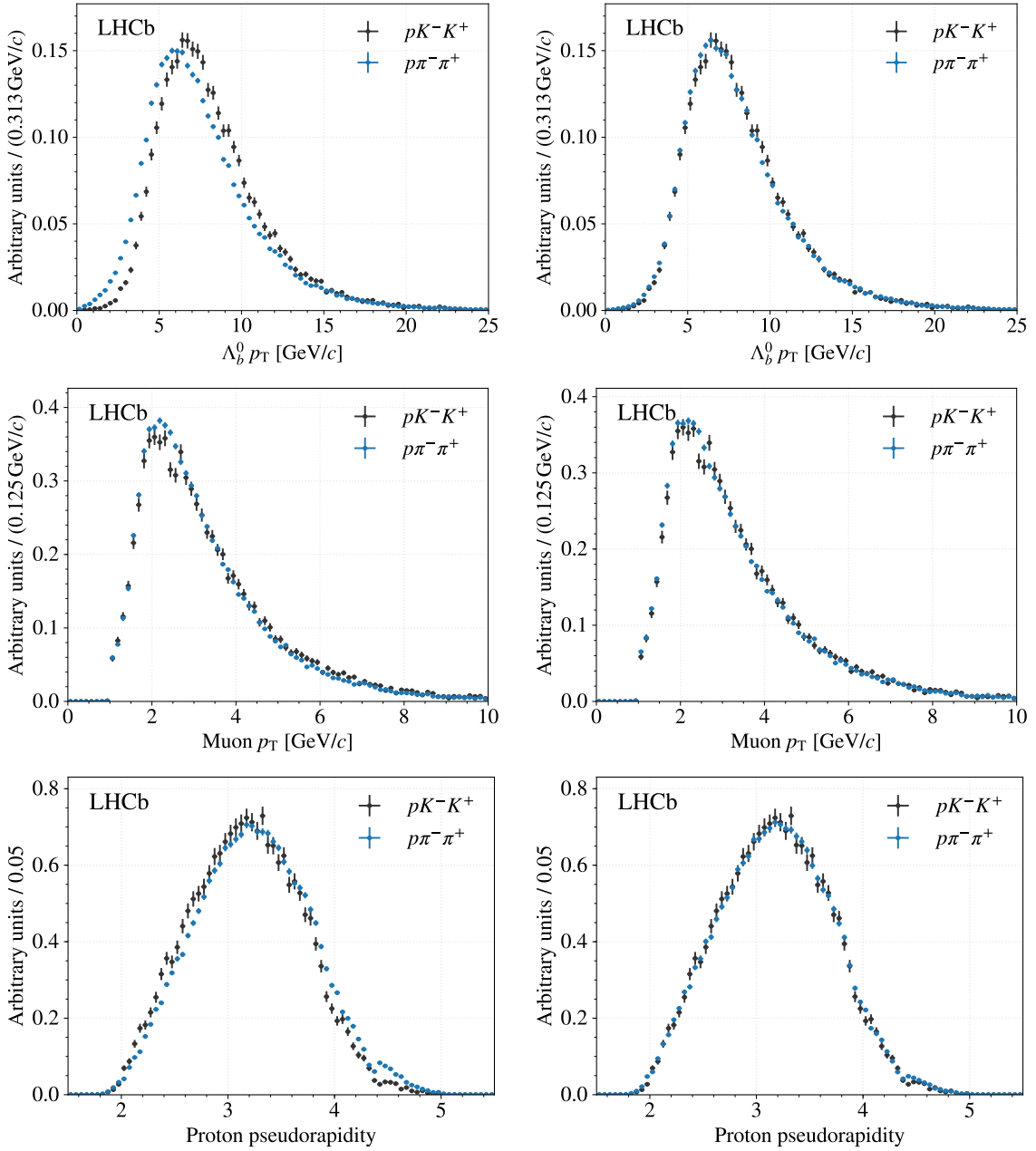


Figure 2. Background-subtracted distributions of the Λ_b^0 candidate transverse momentum (top row), the muon candidate transverse momentum (middle row), and the proton candidate pseudorapidity (bottom row) both before (left column) and after (right column) weighting the $p\pi^-\pi^+$ sample (blue points) to match the pK^-K^+ sample (black points). The data are summed across all data-taking conditions.

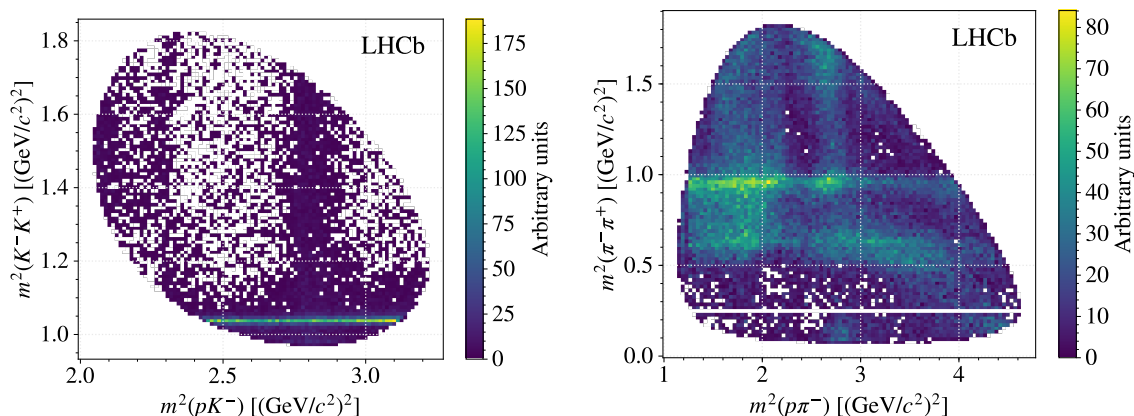


Figure 3. Background-subtracted and efficiency-corrected $\Lambda_c^+ \rightarrow pK^-K^+$ (left) and $\Lambda_c^+ \rightarrow p\pi^-\pi^+$ (right) data in the $m^2(ph^-)-m^2(h^-h^+)$ plane, integrated across all data-taking subsamples. The pK^-K^+ data feature a prominent $\phi \rightarrow K^-K^+$ component, whilst the $p\pi^-\pi^+$ data exhibit $\rho(770)/\omega(782) \rightarrow \pi^-\pi^+$ and $f_0(980) \rightarrow \pi^-\pi^+$ components.

6 Systematic effects

To evaluate possible biases on the measurement of $\Delta A_{CP}^{\text{wgt}}$ due to systematic effects, several studies are performed and deviations from the nominal results are computed. Statistically significant deviations are assigned to the measurement as systematic uncertainties.

The model used in the simultaneous χ^2 fit, described in section 4, is derived empirically, and there may be other models which described the data similarly well. Variations of the choice of background model are found to have a negligible effect on the measurement of $\Delta A_{CP}^{\text{wgt}}$, however different signal models can change the results significantly. To assess an associated systematic uncertainty based on the choice of signal model, the signal Λ_c^+ and $\bar{\Lambda}_c^-$ yields are determined using the method of sideband subtraction. Here, data from the regions on either side of the Λ_c^\pm signal peak are assumed to be linearly distributed and are used to approximate the background yield in the peak region. Given that the data used for sideband subtraction are the same as for the nominal χ^2 fit, the measurements using the two techniques are assumed to be fully correlated, such that even small differences between them are statistically significant. On the average of $\Delta A_{CP}^{\text{wgt}}$, taken across all data-taking conditions, a difference of 0.2% is seen with respect to the average of the results using the full fit, and this difference is assigned as a systematic uncertainty.

The kinematic weighting procedure defined in section 5 can only equalise the $pK^-K^+\mu^-$ and $p\pi^-\pi^+\mu^-$ kinematics approximately, and so residual differences will remain. These differences can cause a bias on $\Delta A_{CP}^{\text{wgt}}$, with a size depending on the size of the relevant asymmetry. Measurements of the Λ_b^0 production asymmetry and the muon, kaon, and pion detection asymmetries using LHCb data exist [5, 8–10], and estimates of the proton detection asymmetry using simulated events have been used previously [8], and so the measurement of $\Delta A_{CP}^{\text{wgt}}$ can be corrected for directly. The correction is found to be less than one per mille, but with a relative uncertainty of 20%, and so a systematic uncertainty of 0.1% is assigned to $\Delta A_{CP}^{\text{wgt}}$.

Source	Uncertainty [%]
Fit signal model	0.20
Fit background model	—
Residual asymmetries	0.10
Limited simulated sample size	0.57
Prompt Λ_c^+	—
Total	0.61

Table 2. Systematic uncertainties on $\Delta A_{CP}^{\text{wgt}}$ and their magnitudes. The dash indicates that the uncertainty is assessed to be negligible.

The limited size of the simulated sample results in a statistical uncertainty on the efficiencies taken from the phase space efficiency model. The size of this uncertainty is evaluated by resampling the simulated data 500 times, each time building a new model and computing the efficiencies of the data using that model. The simultaneous χ^2 fit to measure $A_{\text{raw}}(f)$ is then performed for each set of efficiencies, resulting in a spread of values of $\Delta A_{CP}^{\text{wgt}}$ with a standard deviation of 0.57%, which is taken as the systematic uncertainty due to the limited simulated sample size.

Due to the presence of Λ_c^+ decays originating from sources other than $\Lambda_b^0 \rightarrow \Lambda_c^+ \mu^- X$ decays, such as directly from the PV or from other b -hadron decays, the measurement may be biased, as such sources can carry different experimental asymmetries. The composition of the data sample is inferred from the reconstructed Λ_b^0 mass and from the impact parameter distribution of the Λ_c^+ vertex. The latter is seen to be consistent with that for Λ_c^+ produced exclusively in b -hadron decays, whilst the former is consistent between pK^-K^+ and $p\pi^-\pi^+$ samples, such that asymmetries from other sources will cancel in $\Delta A_{CP}^{\text{wgt}}$. Any associated systematic uncertainty is assumed to be negligible.

The total systematic uncertainty is found to be 0.61%, computed as the sum in quadrature of the individual uncertainties. These are assumed to be uncorrelated and are summarised in table 2.

7 Results

The value of $A_{\text{raw}}(f)$ is found for each final state and data-taking condition separately, and for a given centre-of-mass energy is taken as the arithmetic average of the polarity-dependent measurements. The average across $\sqrt{s} = 7$ TeV and 8 TeV is made by weighting the measurements by their variances. The asymmetries for pK^-K^+ and $p\pi^-\pi^+$ are measured to be

$$\begin{aligned}
 A_{\text{raw}}(pK^-K^+) &= (3.72 \pm 0.78) \%, \\
 A_{\text{raw}}^{\text{wgt}}(p\pi^-\pi^+) &= (3.42 \pm 0.47) \%.
 \end{aligned}$$

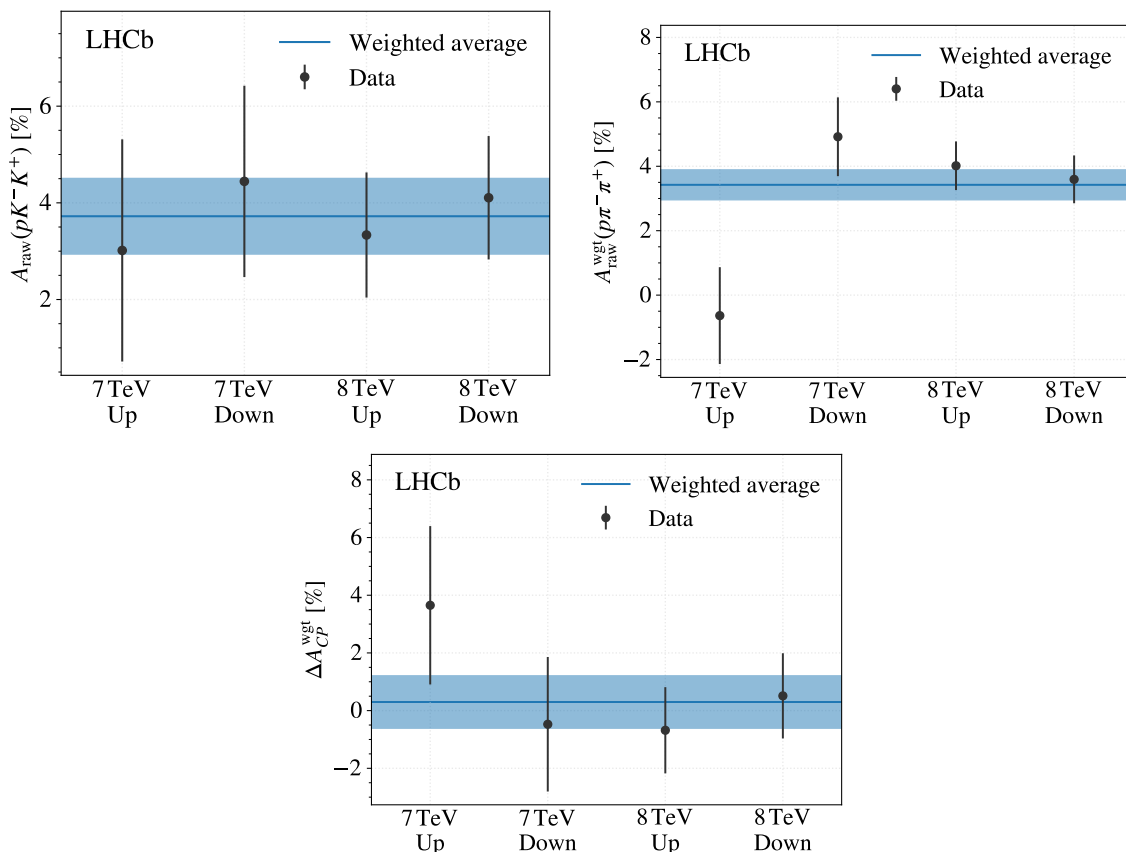


Figure 4. Values of and statistical uncertainties on the asymmetries $A_{\text{raw}}(pK^-K^+)$ (top left), $A_{\text{raw}}^{\text{wgt}}(p\pi^-\pi^+)$ (top right), and $\Delta A_{CP}^{\text{wgt}}$ (bottom centre), for the four data subsamples (two centre-of-mass energies, 7 and 8 TeV, and two polarities of the dipole magnet, up and down). For each asymmetry, the average of the four data points, as described in the text, is also shown, where the band indicates the uncertainty.

where the uncertainties are statistical and take into account the reduction in statistical power due to the weighting. The difference is

$$\Delta A_{CP}^{\text{wgt}} = (0.30 \pm 0.91 \pm 0.61)\%$$

where the first uncertainty is statistical and the second is systematic. The measurements of $A_{\text{raw}}(pK^-K^+)$, $A_{\text{raw}}^{\text{wgt}}(p\pi^-\pi^+)$, and $\Delta A_{CP}^{\text{wgt}}$ as a function of data-taking conditions are presented in figure 4.

8 Summary

The raw CP asymmetries in the decays $\Lambda_c^+ \rightarrow pK^-K^+$ and $p\pi^-\pi^+$ are measured using $\Lambda_b^0 \rightarrow \Lambda_c^+ \mu^- X$ decays. Kinematics in the $p\pi^-\pi^+$ data are weighted to match those in the pK^-K^+ data, such that the effect of experimental asymmetries on the CP asymmetry parameter $\Delta A_{CP}^{\text{wgt}}$ is negligible. Acceptance, reconstruction, and selection efficiencies across

the five-dimensional ph^-h^+ phase space are corrected for. Systematic effects arising from the mass distribution modelling, imperfect kinematic weighting, finite simulated sample size, and the inclusion of Λ_c^+ decays from sources other than $\Lambda_b^0 \rightarrow \Lambda_c^+ \mu^- X$ decays are considered. The total systematic uncertainty assigned to these effects is smaller than the statistical uncertainty on $\Delta A_{CP}^{\text{wgt}}$, whose central value is measured to be consistent with zero.

This analysis constitutes the first measurement of a CP violation parameter in three-body Λ_c^+ decays, but more data is required to match the sensitivity of similar measurements using charm mesons. Further studies into the structure of the ph^-h^+ phase space, across which CP -violating effects may strongly vary, would be beneficial as input to theoretical calculations.

Acknowledgments

We express our gratitude to our colleagues in the CERN accelerator departments for the excellent performance of the LHC. We thank the technical and administrative staff at the LHCb institutes. We acknowledge support from CERN and from the national agencies: CAPES, CNPq, FAPERJ and FINEP (Brazil); MOST and NSFC (China); CNRS/IN2P3 (France); BMBF, DFG and MPG (Germany); INFN (Italy); NWO (The Netherlands); MNiSW and NCN (Poland); MEN/IFA (Romania); MinES and FASO (Russia); MinECo (Spain); SNSF and SER (Switzerland); NASU (Ukraine); STFC (United Kingdom); NSF (U.S.A.). We acknowledge the computing resources that are provided by CERN, IN2P3 (France), KIT and DESY (Germany), INFN (Italy), SURF (The Netherlands), PIC (Spain), GridPP (United Kingdom), RRCKI and Yandex LLC (Russia), CSCS (Switzerland), IFIN-HH (Romania), CBPF (Brazil), PL-GRID (Poland) and OSC (U.S.A.). We are indebted to the communities behind the multiple open-source software packages on which we depend. Individual groups or members have received support from AvH Foundation (Germany), EPLANET, Marie Skłodowska-Curie Actions and ERC (European Union), ANR, Labex P2IO and OCEVU, and Région Auvergne-Rhône-Alpes (France), RFBR, RSF and Yandex LLC (Russia), GVA, XuntaGal and GENCAT (Spain), Herchel Smith Fund, the Royal Society, the English-Speaking Union and the Leverhulme Trust (United Kingdom).

Open Access. This article is distributed under the terms of the Creative Commons Attribution License ([CC-BY 4.0](https://creativecommons.org/licenses/by/4.0/)), which permits any use, distribution and reproduction in any medium, provided the original author(s) and source are credited.

References

- [1] M.B. Gavela, P. Hernández, J. Orloff and O. Pène, *Standard Model CP-violation and baryon asymmetry*, *Mod. Phys. Lett. A* **9** (1994) 795 [[hep-ph/9312215](#)] [[INSPIRE](#)].
- [2] PARTICLE DATA GROUP collaboration, C. Patrignani et al., *Review of particle physics*, *Chin. Phys. C* **40** (2016) 100001 [[INSPIRE](#)].
- [3] HFLAV collaboration, Y. Amhis et al., *Averages of b-hadron, c-hadron and τ -lepton properties as of summer 2016*, *Eur. Phys. J. C* **77** (2017) 895 [[arXiv:1612.07233](#)] [[INSPIRE](#)].

- [4] LHCb collaboration, *Measurement of matter-antimatter differences in beauty baryon decays*, *Nature Phys.* **13** (2017) 391 [[arXiv:1609.05216](#)] [[INSPIRE](#)].
- [5] LHCb collaboration, *Measurement of CP asymmetry in $D^0 \rightarrow K^- K^+$ and $D^0 \rightarrow \pi^- \pi^+$ decays*, *JHEP* **07** (2014) 041 [[arXiv:1405.2797](#)] [[INSPIRE](#)].
- [6] LHCb collaboration, *Measurement of the difference of time-integrated CP asymmetries in $D^0 \rightarrow K^- K^+$ and $D^0 \rightarrow \pi^- \pi^+$ decays*, *Phys. Rev. Lett.* **116** (2016) 191601 [[arXiv:1602.03160](#)] [[INSPIRE](#)].
- [7] I.I. Bigi, *Probing CP asymmetries in charm baryons decays*, [arXiv:1206.4554](#) [[INSPIRE](#)].
- [8] LHCb collaboration, *Study of the production of Λ_b^0 and \bar{B}^0 hadrons in pp collisions and first measurement of the $\Lambda_b^0 \rightarrow J/\psi p K^-$ branching fraction*, *Chin. Phys. C* **40** (2016) 011001 [[arXiv:1509.00292](#)] [[INSPIRE](#)].
- [9] LHCb collaboration, *Measurement of the CP asymmetry in B_s^0 - \bar{B}_s^0 mixing*, *Phys. Rev. Lett.* **117** (2016) 061803 [*Addendum ibid.* **118** (2017) 129903] [[arXiv:1605.09768](#)] [[INSPIRE](#)].
- [10] LHCb collaboration, *Measurement of the $D_s^+ D_s^-$ production asymmetry in 7 TeV pp collisions*, *Phys. Lett. B* **713** (2012) 186 [[arXiv:1205.0897](#)] [[INSPIRE](#)].
- [11] E791 collaboration, E.M. Aitala et al., *Multidimensional resonance analysis of $\Lambda_c^+ \rightarrow p K^- \pi^+$* , *Phys. Lett. B* **471** (2000) 449 [[hep-ex/9912003](#)] [[INSPIRE](#)].
- [12] LHCb collaboration, *The LHCb detector at the LHC*, 2008 *JINST* **3** S08005 [[INSPIRE](#)].
- [13] LHCb collaboration, *LHCb detector performance*, *Int. J. Mod. Phys. A* **30** (2015) 1530022 [[arXiv:1412.6352](#)] [[INSPIRE](#)].
- [14] V.V. Gligorov and M. Williams, *Efficient, reliable and fast high-level triggering using a bonsai boosted decision tree*, 2013 *JINST* **8** P02013 [[arXiv:1210.6861](#)] [[INSPIRE](#)].
- [15] P. Koppenburg, *Statistical biases in measurements with multiple candidates*, [arXiv:1703.01128](#) [[INSPIRE](#)].
- [16] T. Sjöstrand, S. Mrenna and P.Z. Skands, *A brief introduction to PYTHIA 8.1*, *Comput. Phys. Commun.* **178** (2008) 852 [[arXiv:0710.3820](#)] [[INSPIRE](#)].
- [17] T. Sjöstrand, S. Mrenna and P.Z. Skands, *PYTHIA 6.4 physics and manual*, *JHEP* **05** (2006) 026 [[hep-ph/0603175](#)] [[INSPIRE](#)].
- [18] LHCb collaboration, *Handling of the generation of primary events in Gauss, the LHCb simulation framework*, *J. Phys. Conf. Ser.* **331** (2011) 032047 [[INSPIRE](#)].
- [19] D.J. Lange, *The EvtGen particle decay simulation package*, *Nucl. Instrum. Meth. A* **462** (2001) 152 [[INSPIRE](#)].
- [20] P. Golonka and Z. Was, *PHOTOS Monte Carlo: a precision tool for QED corrections in Z and W decays*, *Eur. Phys. J. C* **45** (2006) 97 [[hep-ph/0506026](#)] [[INSPIRE](#)].
- [21] J. Allison et al., *GEANT4 developments and applications*, *IEEE Trans. Nucl. Sci.* **53** (2006) 270 [[INSPIRE](#)].
- [22] GEANT4 collaboration, S. Agostinelli et al., *GEANT4: a simulation toolkit*, *Nucl. Instrum. Meth. A* **506** (2003) 250 [[INSPIRE](#)].
- [23] M. Clemencic et al., *The LHCb simulation application, Gauss: design, evolution and experience*, *J. Phys. Conf. Ser.* **331** (2011) 032023 [[INSPIRE](#)].

- [24] M. Pivk and F.R. Le Diberder, *SPlot: a statistical tool to unfold data distributions*, *Nucl. Instrum. Meth. A* **555** (2005) 356 [[physics/0402083](#)] [[INSPIRE](#)].
- [25] J.H. Friedman, *Greedy function approximation: a gradient boosting machine*, *Ann. Statist.* **29** (2000) 1189.
- [26] J.H. Friedman, *Stochastic gradient boosting*, *Computat. Statist. Data Anal.* **38** (2002) 367.
- [27] A. Rogozhnikov, *Reweighting with boosted decision trees*, *J. Phys. Conf. Ser.* **762** (2016) 012036 [[arXiv:1608.05806](#)] [[INSPIRE](#)].

The LHCb collaboration

R. Aaij⁴⁰, B. Adeva³⁹, M. Adinolfi⁴⁸, Z. Ajaltouni⁵, S. Akar⁵⁹, J. Albrecht¹⁰, F. Alessio⁴⁰, M. Alexander⁵³, A. Alfonso Alberio³⁸, S. Ali⁴³, G. Alkhazov³¹, P. Alvarez Cartelle⁵⁵, A.A. Alves Jr⁵⁹, S. Amato², S. Amerio²³, Y. Amhis⁷, L. An³, L. Anderlini¹⁸, G. Andreassi⁴¹, M. Andreotti^{17,g}, J.E. Andrews⁶⁰, R.B. Appleby⁵⁶, F. Archilli⁴³, P. d'Argent¹², J. Arnau Romeu⁶, A. Artamonov³⁷, M. Artuso⁶¹, E. Aslanides⁶, M. Atzeni⁴², G. Auriemma²⁶, M. Baalouch⁵, I. Babuschkin⁵⁶, S. Bachmann¹², J.J. Back⁵⁰, A. Badalov^{38,m}, C. Baesso⁶², S. Baker⁵⁵, V. Balagura^{7,b}, W. Baldini¹⁷, A. Baranov³⁵, R.J. Barlow⁵⁶, C. Barschel⁴⁰, S. Barsuk⁷, W. Barter⁵⁶, F. Baryshnikov³², V. Batozskaya²⁹, V. Battista⁴¹, A. Bay⁴¹, L. Beaucourt⁴, J. Beddow⁵³, F. Bedeschi²⁴, I. Bediaga¹, A. Beiter⁶¹, L.J. Bel⁴³, N. Bely⁶³, V. Bellec⁴¹, N. Belloli^{21,i}, K. Belous³⁷, I. Belyaev^{32,40}, E. Ben-Haim⁸, G. Bencivenni¹⁹, S. Benson⁴³, S. Beranek⁹, A. Berezhnoy³³, R. Bernet⁴², D. Berninghoff¹², E. Bertholet⁸, A. Bertolin²³, C. Betancourt⁴², F. Betti¹⁵, M.O. Bettler⁴⁰, M. van Beuzekom⁴³, Ia. Bezshyiko⁴², S. Bifani⁴⁷, P. Billoir⁸, A. Birnkraut¹⁰, A. Bizzeti^{18,u}, M. Bjørn⁵⁷, T. Blake⁵⁰, F. Blanc⁴¹, S. Blusk⁶¹, V. Bocci²⁶, T. Boettcher⁵⁸, A. Bondar^{36,w}, N. Bondar³¹, I. Bordyuzhin³², S. Borghi^{56,40}, M. Borisyak³⁵, M. Borsato³⁹, F. Bossu⁷, M. Boubdir⁹, T.J.V. Bowcock⁵⁴, E. Bowen⁴², C. Bozzi^{17,40}, S. Braun¹², J. Brodzicka²⁷, D. Brundu¹⁶, E. Buchanan⁴⁸, C. Burr⁵⁶, A. Bursche^{16,f}, J. Buytaert⁴⁰, W. Byczynski⁴⁰, S. Cadeddu¹⁶, H. Cai⁶⁴, R. Calabrese^{17,g}, R. Calladine⁴⁷, M. Calvi^{21,i}, M. Calvo Gomez^{38,m}, A. Camboni^{38,m}, P. Campana¹⁹, D.H. Campora Perez⁴⁰, L. Capriotti⁵⁶, A. Carbone^{15,e}, G. Carboni^{25,j}, R. Cardinale^{20,h}, A. Cardini¹⁶, P. Carniti^{21,i}, L. Carson⁵², K. Carvalho Akiba², G. Casse⁵⁴, L. Cassina²¹, M. Cattaneo⁴⁰, G. Cavallero^{20,40,h}, R. Cenci^{24,t}, D. Chamont⁷, M.G. Chapman⁴⁸, M. Charles⁸, Ph. Charpentier⁴⁰, G. Chatzikonstantinidis⁴⁷, M. Chefdeville⁴, S. Chen¹⁶, S.F. Cheung⁵⁷, S.-G. Chitic⁴⁰, V. Chobanova³⁹, M. Chrzaszcz⁴², A. Chubykin³¹, P. Ciambone¹⁹, X. Cid Vidal³⁹, G. Ciezarek⁴⁰, P.E.L. Clarke⁵², M. Clemencic⁴⁰, H.V. Cliff⁴⁹, J. Closier⁴⁰, V. Coco⁴⁰, J. Cogan⁶, E. Cogneras⁵, V. Cogoni^{16,f}, L. Cojocariu³⁰, P. Collins⁴⁰, T. Colombo⁴⁰, A. Comerma-Montells¹², A. Contu¹⁶, G. Coombs⁴⁰, S. Coquereau³⁸, G. Corti⁴⁰, M. Corvo^{17,g}, C.M. Costa Sobral⁵⁰, B. Couturier⁴⁰, G.A. Cowan⁵², D.C. Craik⁵⁸, A. Crocombe⁵⁰, M. Cruz Torres¹, R. Currie⁵², C. D'Ambrosio⁴⁰, F. Da Cunha Marinho², C.L. Da Silva⁷³, E. Dall'Occo⁴³, J. Dalseno⁴⁸, A. Davis³, O. De Aguiar Francisco⁴⁰, K. De Bruyn⁴⁰, S. De Capua⁵⁶, M. De Cian¹², J.M. De Miranda¹, L. De Paula², M. De Serio^{14,d}, P. De Simone¹⁹, C.T. Dean⁵³, D. Decamp⁴, L. Del Buono⁸, H.-P. Dembinski¹¹, M. Demmer¹⁰, A. Dendek²⁸, D. Derkach³⁵, O. Deschamps⁵, F. Dettori⁵⁴, B. Dey⁶⁵, A. Di Canto⁴⁰, P. Di Nezza¹⁹, H. Dijkstra⁴⁰, F. Dordei⁴⁰, M. Dorigo⁴⁰, A. Dosil Suárez³⁹, L. Douglas⁵³, A. Dovbnya⁴⁵, K. Dreimanis⁵⁴, L. Dufour⁴³, G. Dujany⁸, P. Durante⁴⁰, J.M. Durham⁷³, D. Dutta⁵⁶, R. Dzhelyadin³⁷, M. Dziewiecki¹², A. Dziurda⁴⁰, A. Dzyuba³¹, S. Easo⁵¹, M. Ebert⁵², U. Egede⁵⁵, V. Egorychev³², S. Eidelman^{36,w}, S. Eisenhardt⁵², U. Eitschberger¹⁰, R. Ekelhof¹⁰, L. Eklund⁵³, S. Ely⁶¹, S. Esen¹², H.M. Evans⁴⁹, T. Evans⁵⁷, A. Falabella¹⁵, N. Farley⁴⁷, S. Farry⁵⁴, D. Fazzini^{21,i}, L. Federici²⁵, D. Ferguson⁵², G. Fernandez³⁸, P. Fernandez Declara⁴⁰, A. Fernandez Prieto³⁹, F. Ferrari¹⁵, L. Ferreira Lopes⁴¹, F. Ferreira Rodrigues², M. Ferro-Luzzi⁴⁰, S. Filippov³⁴, R.A. Fini¹⁴, M. Fiorini^{17,g}, M. Firlej²⁸, C. Fitzpatrick⁴¹, T. Fiutowski²⁸, F. Fleuret^{7,b}, M. Fontana^{16,40}, F. Fontanelli^{20,h}, R. Forty⁴⁰, V. Franco Lima⁵⁴, M. Frank⁴⁰, C. Frei⁴⁰, J. Fu^{22,q}, W. Funk⁴⁰, E. Furfaro^{25,j}, C. Färber⁴⁰, E. Gabriel⁵², A. Gallas Torreira³⁹, D. Galli^{15,e}, S. Gallorini²³, S. Gambetta⁵², M. Gandelman², P. Gandini²², Y. Gao³, L.M. Garcia Martin⁷¹, J. García Pardiñas³⁹, J. Garra Tico⁴⁹, L. Garrido³⁸, D. Gascon³⁸, C. Gaspar⁴⁰, L. Gavardi¹⁰, G. Gazzoni⁵, D. Gerick¹², E. Gersabeck⁵⁶, M. Gersabeck⁵⁶, T. Gershon⁵⁰, Ph. Ghez⁴, S. Gianì⁴¹, V. Gibson⁴⁹, O.G. Girard⁴¹, L. Giubega³⁰, K. Gizdov⁵², V.V. Gligorov⁸, D. Golubkov³², A. Golutvin^{55,69,y}, A. Gomes^{1,a}, I.V. Gorelov³³,

C. Gotti^{21,i}, E. Govorkova⁴³, J.P. Grabowski¹², R. Graciani Diaz³⁸, L.A. Granado Cardoso⁴⁰,
 E. Graugés³⁸, E. Graverini⁴², G. Graziani¹⁸, A. Grecu³⁰, R. Greim⁹, P. Griffith¹⁶, L. Grillo⁵⁶,
 L. Gruber⁴⁰, B.R. Gruberg Cazon⁵⁷, O. Grünberg⁶⁷, E. Gushchin³⁴, Yu. Guz³⁷, T. Gys⁴⁰,
 C. Göbel⁶², T. Hadavizadeh⁵⁷, C. Hadjivasiliou⁵, G. Haefeli⁴¹, C. Haen⁴⁰, S.C. Haines⁴⁹,
 B. Hamilton⁶⁰, X. Han¹², T.H. Hancock⁵⁷, S. Hansmann-Menzemer¹², N. Harnew⁵⁷,
 S.T. Harnew⁴⁸, C. Hasse⁴⁰, M. Hatch⁴⁰, J. He⁶³, M. Hecker⁵⁵, K. Heinicke¹⁰, A. Heister⁹,
 K. Hennessy⁵⁴, P. Henrard⁵, L. Henry⁷¹, E. van Herwijnen⁴⁰, M. Heß⁶⁷, A. Hicheur², D. Hill⁵⁷,
 P.H. Hopchev⁴¹, W. Hu⁶⁵, W. Huang⁶³, Z.C. Huard⁵⁹, W. Hulsbergen⁴³, T. Humair⁵⁵,
 M. Hushchyn³⁵, D. Hutchcroft⁵⁴, P. Ibis¹⁰, M. Idzik²⁸, P. Ilten⁴⁷, R. Jacobsson⁴⁰, J. Jalocha⁵⁷,
 E. Jans⁴³, A. Jawahery⁶⁰, F. Jiang³, M. John⁵⁷, D. Johnson⁴⁰, C.R. Jones⁴⁹, C. Joram⁴⁰,
 B. Jost⁴⁰, N. Jurik⁵⁷, S. Kandybei⁴⁵, M. Karacson⁴⁰, J.M. Kariuki⁴⁸, S. Karodia⁵³, N. Kazeev³⁵,
 M. Kecke¹², F. Keizer⁴⁹, M. Kelsey⁶¹, M. Kenzie⁴⁹, T. Ketel⁴⁴, E. Khairullin³⁵, B. Khanji¹²,
 C. Khurewathanakul⁴¹, T. Kirn⁹, S. Klaver¹⁹, K. Klimaszewski²⁹, T. Klimovich¹¹, S. Koliiev⁴⁶,
 M. Kolpin¹², R. Kopečna¹², P. Koppenburg⁴³, A. Kosmyntseva³², S. Kotriakhova³¹, M. Kozeiha⁵,
 L. Kravchuk³⁴, M. Krepš⁵⁰, F. Kress⁵⁵, P. Krokovny^{36,w}, W. Krzemien²⁹, W. Kucewicz^{27,l},
 M. Kucharczyk²⁷, V. Kudryavtsev^{36,w}, A.K. Kuonen⁴¹, T. Kvaratskheliya^{32,40}, D. Lacarrere⁴⁰,
 G. Lafferty⁵⁶, A. Lai¹⁶, G. Lanfranchi¹⁹, C. Langenbruch⁹, T. Latham⁵⁰, C. Lazzeroni⁴⁷,
 R. Le Gac⁶, A. Leflat^{33,40}, J. Lefrançois⁷, R. Lefevre⁵, F. Lemaître⁴⁰, E. Lemos Cid³⁹, O. Leroy⁶,
 T. Lesiak²⁷, B. Leverington¹², P.-R. Li⁶³, T. Li³, Y. Li⁷, Z. Li⁶¹, X. Liang⁶¹, T. Likhomanenko⁶⁸,
 R. Lindner⁴⁰, F. Lionetto⁴², V. Lisovskyi⁷, X. Liu³, D. Loh⁵⁰, A. Loi¹⁶, I. Longstaff⁵³,
 J.H. Lopes², D. Lucchesi^{23,o}, M. Lucio Martinez³⁹, H. Luo⁵², A. Lupato²³, E. Luppi^{17,g},
 O. Lupton⁴⁰, A. Lusiani²⁴, X. Lyu⁶³, F. Machefert⁷, F. Maciuc³⁰, V. Macko⁴¹, P. Mackowiak¹⁰,
 S. Maddrell-Mander⁴⁸, O. Maev^{31,40}, K. Maguire⁵⁶, D. Maisuzenko³¹, M.W. Majewski²⁸,
 S. Malde⁵⁷, B. Malecki²⁷, A. Malinin⁶⁸, T. Maltsev^{36,w}, G. Manca^{16,f}, G. Mancinelli⁶,
 D. Marangotto^{22,q}, J. Maratas^{5,v}, J.F. Marchand⁴, U. Marconi¹⁵, C. Marin Benito³⁸,
 M. Marinangeli⁴¹, P. Marino⁴¹, J. Marks¹², G. Martellotti²⁶, M. Martin⁶, M. Martinelli⁴¹,
 D. Martinez Santos³⁹, F. Martinez Vidal⁷¹, A. Massafferri¹, R. Mateu⁴⁰, A. Mathad⁵⁰,
 Z. Mathe⁴⁰, C. Matteuzzi²¹, A. Mauri⁴², E. Maurice^{7,b}, B. Maurin⁴¹, A. Mazurov⁴⁷,
 M. McCann^{55,40}, A. McNab⁵⁶, R. McNulty¹³, J.V. Mead⁵⁴, B. Meadows⁵⁹, C. Meaux⁶, F. Meier¹⁰,
 N. Meinert⁶⁷, D. Melnychuk²⁹, M. Merk⁴³, A. Merli^{22,40,g}, E. Michielin²³, D.A. Milanes⁶⁶,
 E. Millard⁵⁰, M.-N. Minard⁴, L. Minzoni¹⁷, D.S. Mitzel¹², A. Mogini⁸, J. Molina Rodriguez¹,
 T. Mombächer¹⁰, I.A. Monroy⁶⁶, S. Monteil⁵, M. Morandin²³, M.J. Morello^{24,t}, O. Morgunova⁶⁸,
 J. Moron²⁸, A.B. Morris⁵², R. Mountain⁶¹, F. Muheim⁵², M. Mulder⁴³, D. Müller⁵⁶, J. Müller¹⁰,
 K. Müller⁴², V. Müller¹⁰, P. Naik⁴⁸, T. Nakada⁴¹, R. Nandakumar⁵¹, A. Nandi⁵⁷, I. Nasteva²,
 M. Needham⁵², N. Neri^{22,40}, S. Neubert¹², N. Neufeld⁴⁰, M. Neuner¹², T.D. Nguyen⁴¹,
 C. Nguyen-Mau^{41,n}, S. Nieswand⁹, R. Niet¹⁰, N. Nikitin³³, T. Nikodem¹², A. Nogay⁶⁸,
 D.P. O'Hanlon⁵⁰, A. Oblakowska-Mucha²⁸, V. Obraztsov³⁷, S. Ogilvy¹⁹, R. Oldeman^{16,f},
 C.J.G. Onderwater⁷², A. Ossowska²⁷, J.M. Otalora Goicochea², P. Owen⁴², A. Oyanguren⁷¹,
 P.R. Pais⁴¹, A. Palano¹⁴, M. Palutan^{19,40}, A. Papanestis⁵¹, M. Pappagallo⁵², L.L. Pappalardo^{17,g},
 W. Parker⁶⁰, C. Parkes⁵⁶, G. Passaleva^{18,40}, A. Pastore^{14,d}, M. Patel⁵⁵, C. Patrignani^{15,e},
 A. Pearce⁴⁰, A. Pellegrino⁴³, G. Penso²⁶, M. Pepe Altarelli⁴⁰, S. Perazzini⁴⁰, D. Pereima³²,
 P. Perret⁵, L. Pescatore⁴¹, K. Petridis⁴⁸, A. Petrolini^{20,h}, A. Petrov⁶⁸, M. Petruzzio^{22,q},
 E. Picatoste Olloqui³⁸, B. Pietrzyk⁴, G. Pietrzyk⁴¹, M. Piekies²⁷, D. Pinci²⁶, F. Pisani⁴⁰,
 A. Pistone^{20,h}, A. Piucci¹², V. Placinta³⁰, S. Playfer⁵², M. Plo Casasus³⁹, F. Polci⁸,
 M. Poli Lener¹⁹, A. Poluektov⁵⁰, I. Polyakov⁶¹, E. Polcarpo², G.J. Pomery⁴⁸, S. Ponce⁴⁰,
 A. Popov³⁷, D. Popov^{11,40}, S. Poslavskii³⁷, C. Potterat², E. Price⁴⁸, J. Prisciandaro³⁹,
 C. Prouve⁴⁸, V. Pugatch⁴⁶, A. Puig Navarro⁴², H. Pullen⁵⁷, G. Punzi^{24,p}, W. Qian⁵⁰, J. Qin⁶³,
 R. Quagliani⁸, B. Quintana⁵, B. Rachwal²⁸, J.H. Rademacker⁴⁸, M. Rama²⁴, M. Ramos Pernas³⁹,

M.S. Rangel², I. Raniuk^{45,†}, F. Ratnikov^{35,x}, G. Raven⁴⁴, M. Ravonel Salzgeber⁴⁰, M. Reboud⁴, F. Redi⁴¹, S. Reichert¹⁰, A.C. dos Reis¹, C. Remon Alepuz⁷¹, V. Renaudin⁷, S. Ricciardi⁵¹, S. Richards⁴⁸, M. Rihl⁴⁰, K. Rinnert⁵⁴, P. Robbe⁷, A. Robert⁸, A.B. Rodrigues⁴¹, E. Rodrigues⁵⁹, J.A. Rodriguez Lopez⁶⁶, A. Rogozhnikov³⁵, S. Roiser⁴⁰, A. Rollings⁵⁷, V. Romanovskiy³⁷, A. Romero Vidal^{39,40}, M. Rotondo¹⁹, M.S. Rudolph⁶¹, T. Ruf⁴⁰, P. Ruiz Valls⁷¹, J. Ruiz Vidal⁷¹, J.J. Saborido Silva³⁹, E. Sadykhov³², N. Sagidova³¹, B. Saitta^{16,f}, V. Salustino Guimaraes⁶², C. Sanchez Mayordomo⁷¹, B. Sanmartin Sedes³⁹, R. Santacesaria²⁶, C. Santamarina Rios³⁹, M. Santimaria¹⁹, E. Santovetti^{25,j}, G. Sarpis⁵⁶, A. Sarti^{19,k}, C. Satriano^{26,s}, A. Satta²⁵, D.M. Saunders⁴⁸, D. Savrina^{32,33}, S. Schael⁹, M. Schellenberg¹⁰, M. Schiller⁵³, H. Schindler⁴⁰, M. Schmelling¹¹, T. Schmelzer¹⁰, B. Schmidt⁴⁰, O. Schneider⁴¹, A. Schopper⁴⁰, H.F. Schreiner⁵⁹, M. Schubiger⁴¹, M.H. Schune⁷, R. Schwemmer⁴⁰, B. Sciascia¹⁹, A. Sciubba^{26,k}, A. Semennikov³², E.S. Sepulveda⁸, A. Sergi⁴⁷, N. Serra⁴², J. Serrano⁶, L. Sestini²³, P. Seyfert⁴⁰, M. Shapkin³⁷, I. Shapoval⁴⁵, Y. Shcheglov³¹, T. Shears⁵⁴, L. Shekhtman^{36,w}, V. Shevchenko⁶⁸, B.G. Siddi¹⁷, R. Silva Coutinho⁴², L. Silva de Oliveira², G. Simi^{23,o}, S. Simone^{14,d}, M. Sirendi⁴⁹, N. Skidmore⁴⁸, T. Skwarnicki⁶¹, I.T. Smith⁵², J. Smith⁴⁹, M. Smith⁵⁵, I. Soares Lavra¹, M.D. Sokoloff⁵⁹, F.J.P. Soler⁵³, B. Souza De Paula², B. Spaan¹⁰, P. Spradlin⁵³, S. Sridharan⁴⁰, F. Stagni⁴⁰, M. Stahl¹², S. Stahl⁴⁰, P. Stefko⁴¹, S. Stefkova⁵⁵, O. Steinkamp⁴², S. Stemmler¹², O. Stenyakin³⁷, M. Stepanova³¹, H. Stevens¹⁰, S. Stone⁶¹, B. Storaci⁴², S. Stracka^{24,p}, M.E. Stramaglia⁴¹, M. Straticiu³⁰, U. Straumann⁴², J. Sun³, L. Sun⁶⁴, K. Swientek²⁸, V. Syropoulos⁴⁴, T. Szumlak²⁸, M. Szymanski⁶³, S. T'Jampens⁴, A. Tayduganov⁶, T. Tekampe¹⁰, G. Tellarini^{17,g}, F. Teubert⁴⁰, E. Thomas⁴⁰, J. van Tilburg⁴³, M.J. Tilley⁵⁵, V. Tisserand⁵, M. Tobin⁴¹, S. Tolkar⁴⁹, L. Tomassetti^{17,g}, D. Tonelli²⁴, R. Tourinho Jadallah Aoude¹, E. Tournefier⁴, M. Traill⁵³, M.T. Tran⁴¹, M. Tresch⁴², A. Trisovic⁴⁹, A. Tsaregorodtsev⁶, P. Tsopelas⁴³, A. Tully⁴⁹, N. Tuning^{43,40}, A. Ukleja²⁹, A. Usachov⁷, A. Ustyuzhanin³⁵, U. Uwer¹², C. Vacca^{16,f}, A. Vagner⁷⁰, V. Vagnoni^{15,40}, A. Valassi⁴⁰, S. Valat⁴⁰, G. Valenti¹⁵, R. Vazquez Gomez⁴⁰, P. Vazquez Regueiro³⁹, S. Vecchi¹⁷, M. van Veghel⁴³, J.J. Velthuis⁴⁸, M. Veltri^{18,r}, G. Veneziano⁵⁷, A. Venkateswaran⁶¹, T.A. Verlage⁹, M. Vernet⁵, M. Vesterinen⁵⁷, J.V. Viana Barbosa⁴⁰, D. Vieira⁶³, M. Vieites Diaz³⁹, H. Viemann⁶⁷, X. Vilasis-Cardona^{38,m}, M. Vitti⁴⁹, V. Volkov³³, A. Vollhardt⁴², B. Voneki⁴⁰, A. Vorobyev³¹, V. Vorobyev^{36,w}, C. Voß⁹, J.A. de Vries⁴³, C. Vázquez Sierra⁴³, R. Waldi⁶⁷, J. Walsh²⁴, J. Wang⁶¹, Y. Wang⁶⁵, D.R. Ward⁴⁹, H.M. Wark⁵⁴, N.K. Watson⁴⁷, D. Websdale⁵⁵, A. Weiden⁴², C. Weisser⁵⁸, M. Whitehead⁴⁰, J. Wicht⁵⁰, G. Wilkinson⁵⁷, M. Wilkinson⁶¹, M. Williams⁵⁶, M. Williams⁵⁸, T. Williams⁴⁷, F.F. Wilson^{51,40}, J. Wimberley⁶⁰, M. Winn⁷, J. Wishahi¹⁰, W. Wislicki²⁹, M. Witek²⁷, G. Wormser⁷, S.A. Wotton⁴⁹, K. Wyllie⁴⁰, Y. Xie⁶⁵, M. Xu⁶⁵, Q. Xu⁶³, Z. Xu³, Z. Xu⁴, Z. Yang³, Z. Yang⁶⁰, Y. Yao⁶¹, H. Yin⁶⁵, J. Yu⁶⁵, X. Yuan⁶¹, O. Yushchenko³⁷, K.A. Zarebski⁴⁷, M. Zavertyaev^{11,c}, L. Zhang³, Y. Zhang⁷, A. Zhelezov¹², Y. Zheng⁶³, X. Zhu³, V. Zhukov^{9,33}, J.B. Zonneveld⁵² and S. Zucchelli¹⁵

¹ Centro Brasileiro de Pesquisas Físicas (CBPF), Rio de Janeiro, Brazil

² Universidade Federal do Rio de Janeiro (UFRJ), Rio de Janeiro, Brazil

³ Center for High Energy Physics, Tsinghua University, Beijing, China

⁴ Univ. Grenoble Alpes, Univ. Savoie Mont Blanc, CNRS, IN2P3-LAPP, Annecy, France

⁵ Clermont Université, Université Blaise Pascal, CNRS/IN2P3, LPC, Clermont-Ferrand, France

⁶ Aix Marseille Univ, CNRS/IN2P3, CPPM, Marseille, France

⁷ LAL, Univ. Paris-Sud, CNRS/IN2P3, Université Paris-Saclay, Orsay, France

⁸ LPNHE, Université Pierre et Marie Curie, Université Paris Diderot, CNRS/IN2P3, Paris, France

⁹ I. Physikalisches Institut, RWTH Aachen University, Aachen, Germany

¹⁰ Fakultät Physik, Technische Universität Dortmund, Dortmund, Germany

¹¹ Max-Planck-Institut für Kernphysik (MPIK), Heidelberg, Germany

- 12 *Physikalisches Institut, Ruprecht-Karls-Universität Heidelberg, Heidelberg, Germany*
- 13 *School of Physics, University College Dublin, Dublin, Ireland*
- 14 *Sezione INFN di Bari, Bari, Italy*
- 15 *Sezione INFN di Bologna, Bologna, Italy*
- 16 *Sezione INFN di Cagliari, Cagliari, Italy*
- 17 *Università e INFN, Ferrara, Ferrara, Italy*
- 18 *Sezione INFN di Firenze, Firenze, Italy*
- 19 *Laboratori Nazionali dell'INFN di Frascati, Frascati, Italy*
- 20 *Sezione INFN di Genova, Genova, Italy*
- 21 *Sezione INFN di Milano Bicocca, Milano, Italy*
- 22 *Sezione di Milano, Milano, Italy*
- 23 *Sezione INFN di Padova, Padova, Italy*
- 24 *Sezione INFN di Pisa, Pisa, Italy*
- 25 *Sezione INFN di Roma Tor Vergata, Roma, Italy*
- 26 *Sezione INFN di Roma La Sapienza, Roma, Italy*
- 27 *Henryk Niewodniczanski Institute of Nuclear Physics Polish Academy of Sciences, Kraków, Poland*
- 28 *AGH - University of Science and Technology, Faculty of Physics and Applied Computer Science, Kraków, Poland*
- 29 *National Center for Nuclear Research (NCBJ), Warsaw, Poland*
- 30 *Horia Hulubei National Institute of Physics and Nuclear Engineering, Bucharest-Magurele, Romania*
- 31 *Petersburg Nuclear Physics Institute (PNPI), Gatchina, Russia*
- 32 *Institute of Theoretical and Experimental Physics (ITEP), Moscow, Russia*
- 33 *Institute of Nuclear Physics, Moscow State University (SINP MSU), Moscow, Russia*
- 34 *Institute for Nuclear Research of the Russian Academy of Sciences (INR RAS), Moscow, Russia*
- 35 *Yandex School of Data Analysis, Moscow, Russia*
- 36 *Budker Institute of Nuclear Physics (SB RAS), Novosibirsk, Russia*
- 37 *Institute for High Energy Physics (IHEP), Protvino, Russia*
- 38 *ICCUB, Universitat de Barcelona, Barcelona, Spain*
- 39 *Instituto Galego de Física de Altas Enerxías (IGFAE), Universidade de Santiago de Compostela, Santiago de Compostela, Spain*
- 40 *European Organization for Nuclear Research (CERN), Geneva, Switzerland*
- 41 *Institute of Physics, Ecole Polytechnique Fédérale de Lausanne (EPFL), Lausanne, Switzerland*
- 42 *Physik-Institut, Universität Zürich, Zürich, Switzerland*
- 43 *Nikhef National Institute for Subatomic Physics, Amsterdam, The Netherlands*
- 44 *Nikhef National Institute for Subatomic Physics and VU University Amsterdam, Amsterdam, The Netherlands*
- 45 *NSC Kharkiv Institute of Physics and Technology (NSC KIPT), Kharkiv, Ukraine*
- 46 *Institute for Nuclear Research of the National Academy of Sciences (KINR), Kyiv, Ukraine*
- 47 *University of Birmingham, Birmingham, United Kingdom*
- 48 *H.H. Wills Physics Laboratory, University of Bristol, Bristol, United Kingdom*
- 49 *Cavendish Laboratory, University of Cambridge, Cambridge, United Kingdom*
- 50 *Department of Physics, University of Warwick, Coventry, United Kingdom*
- 51 *STFC Rutherford Appleton Laboratory, Didcot, United Kingdom*
- 52 *School of Physics and Astronomy, University of Edinburgh, Edinburgh, United Kingdom*
- 53 *School of Physics and Astronomy, University of Glasgow, Glasgow, United Kingdom*
- 54 *Oliver Lodge Laboratory, University of Liverpool, Liverpool, United Kingdom*
- 55 *Imperial College London, London, United Kingdom*
- 56 *School of Physics and Astronomy, University of Manchester, Manchester, United Kingdom*
- 57 *Department of Physics, University of Oxford, Oxford, United Kingdom*
- 58 *Massachusetts Institute of Technology, Cambridge, MA, United States*
- 59 *University of Cincinnati, Cincinnati, OH, United States*

- ⁶⁰ *University of Maryland, College Park, MD, United States*
- ⁶¹ *Syracuse University, Syracuse, NY, United States*
- ⁶² *Pontifícia Universidade Católica do Rio de Janeiro (PUC-Rio), Rio de Janeiro, Brazil, associated to ²*
- ⁶³ *University of Chinese Academy of Sciences, Beijing, China, associated to ³*
- ⁶⁴ *School of Physics and Technology, Wuhan University, Wuhan, China, associated to ³*
- ⁶⁵ *Institute of Particle Physics, Central China Normal University, Wuhan, Hubei, China, associated to ³*
- ⁶⁶ *Departamento de Física, Universidad Nacional de Colombia, Bogota, Colombia, associated to ⁸*
- ⁶⁷ *Institut für Physik, Universität Rostock, Rostock, Germany, associated to ¹²*
- ⁶⁸ *National Research Centre Kurchatov Institute, Moscow, Russia, associated to ³²*
- ⁶⁹ *National University of Science and Technology MISIS, Moscow, Russia, associated to ³²*
- ⁷⁰ *National Research Tomsk Polytechnic University, Tomsk, Russia, associated to ³²*
- ⁷¹ *Instituto de Física Corpuscular, Centro Mixto Universidad de Valencia - CSIC, Valencia, Spain, associated to ³⁸*
- ⁷² *Van Swinderen Institute, University of Groningen, Groningen, The Netherlands, associated to ⁴³*
- ⁷³ *Los Alamos National Laboratory (LANL), Los Alamos, United States, associated to ⁶¹*
- ^a *Universidade Federal do Triângulo Mineiro (UFTM), Uberaba-MG, Brazil*
- ^b *Laboratoire Leprince-Ringuet, Palaiseau, France*
- ^c *P.N. Lebedev Physical Institute, Russian Academy of Science (LPI RAS), Moscow, Russia*
- ^d *Università di Bari, Bari, Italy*
- ^e *Università di Bologna, Bologna, Italy*
- ^f *Università di Cagliari, Cagliari, Italy*
- ^g *Università di Ferrara, Ferrara, Italy*
- ^h *Università di Genova, Genova, Italy*
- ⁱ *Università di Milano Bicocca, Milano, Italy*
- ^j *Università di Roma Tor Vergata, Roma, Italy*
- ^k *Università di Roma La Sapienza, Roma, Italy*
- ^l *AGH - University of Science and Technology, Faculty of Computer Science, Electronics and Telecommunications, Kraków, Poland*
- ^m *LIFAELS, La Salle, Universitat Ramon Llull, Barcelona, Spain*
- ⁿ *Hanoi University of Science, Hanoi, Vietnam*
- ^o *Università di Padova, Padova, Italy*
- ^p *Università di Pisa, Pisa, Italy*
- ^q *Università degli Studi di Milano, Milano, Italy*
- ^r *Università di Urbino, Urbino, Italy*
- ^s *Università della Basilicata, Potenza, Italy*
- ^t *Scuola Normale Superiore, Pisa, Italy*
- ^u *Università di Modena e Reggio Emilia, Modena, Italy*
- ^v *Iligan Institute of Technology (IIT), Iligan, Philippines*
- ^w *Novosibirsk State University, Novosibirsk, Russia*
- ^x *National Research University Higher School of Economics, Moscow, Russia*
- ^y *National University of Science and Technology MISIS, Moscow, Russia*
- [†] *Deceased*